Preferred frequency responses to oscillatory inputs in an electrochemical cell model: Linear amplitude and phase resonance

Horacio G. Rotstein

Department of Mathematical Sciences, New Jersey Institute of Technology, Newark, New Jersey 07102, USA

We investigate the dynamic mechanisms of generation of amplitude and phase resonance in a phenomenological electrochemical cell model in response to sinusoidal inputs. We describe how the attributes of the impedance and phase profiles change as the participating physicochemical parameters vary within a range corresponding to the existence of stable nodes and foci in the corresponding autonomous system, thus extending previous work that considered systems close to limit cycle regimes. The method we use permits us to understand how changes in these parameters generate amplifications of the cell's response at the resonant frequency band and captures some important nonlinear effects.

PACS number(s): 05.45.−a, 82.47.−a, 87.19.ln

I. INTRODUCTION

Oscillatory patterns are frequently observed in nonlinear, far from equilibrium, electrochemical (EC) systems under both potentiostatic and galvanostatic conditions [1–5]. While EC oscillations may result from the effects of external controlling mechanisms, recent work has shown that they may also emerge intrinsically due to negative feedback effects in the interfacial electrode kinetics [1]. Specifically, activators, such as electrode potentials or currents, stimulate both their own production, via autocatalytic effects (positive feedback), and the production of inhibitors, such as surface concentrations. The latter repress the production of the activator, thus generating a negative feedback effect.

The effects of external oscillatory forcing on EC cells have been studied in a number of systems [1,6–13]. Typical experimental protocols using electrochemical impedance spectroscopy (ECIS) [2,6–8,14] consist of driving an EC system with a sinusoidal voltage and measuring both the amplitude and phase shift of the resulting oscillatory current response. Together, these two quantities as a function of the input frequency determine the impedance profile of the system, which is a complex function. Following previous work [15] we use the terms impedance (Z) and phase (ϕ) to refer to the impedance amplitude and phase-shift respectively.

Resonance refers to the ability of a dynamical system to exhibit a peak in the impedance profile at a preferred (resonant) frequency [Fig. 1(a1)]. Resonance occurs in RLC circuits but not in RC circuits, which are low-pass filters [Fig. 1(a2)]. In addition, for RC circuits the phase is always an increasing function of the input frequency [Fig. 1(b2)], capturing a delayed response. In contrast, RLC circuits may exhibit *phasonance* (phase-resonance), a zero-phase response at a nonzero (*phasonant*) frequency [Fig. 1(b1)]. The phasonant frequency corresponds to the input frequency at which both input and output are synchronized in phase. For input frequencies below (above) the phasonant frequency the response is advanced (delayed). The resonant and phasonant frequencies coincide for RLC circuits in series but not for RLC circuits in parallel, as EC cells typically are [15]. Linear three-dimensional systems may exhibits an additional impedance extremum (minimum) and zero-crossing phase [16]. These systems are beyond the scope of this paper and will not be discussed further.

In this paper we investigate the resonant properties of a two-dimensional phenomenological model introduced in Ref. [17] to describe the dynamics of an EC cell under potentiostatic conditions. The model consists of two dependent variables, the electrode potential and the surface concentration. Although it is a phenomenological model, it captures the oscillatory behavior typically observed in realistic systems [18], in particular it displays limit cycle oscillations created in a Hopf bifurcation.

It has been proposed that resonance consists of the amplification of an intrinsic oscillatory behavior present in the underlying autonomous system [9–11], which has a nonzero eigenfrequency, also referred to as the intrinsic or natural frequency. One implication of this idea is that the resonant and intrinsic frequencies are equal or not too far apart [11]. While this is the case in some restricted parameter regimes as it occurs in the so-called λ-ω systems (see Appendix A 3), in general, even for two-dimensional systems, resonance and intrinsic oscillations may occur in the absence of each other [15,16]. Moreover, the intrinsic, resonant, and phasonant frequencies do not necessarily coincide.

The impedance and phase profiles can be characterized by a set of attributes (described in detail in Sec. II) including the resonant and phasonant frequencies, the maximum impedance, and the resonance amplitude. The study of the properties of a system's response to oscillatory inputs can be greatly simplified if one evaluates how changes in parameter values affect the set of attributes rather than the full impedance and phase profiles.

Following this approach, in Ref. [15] we have identified the basic mechanisms of generation of resonance and phasonance in two-dimensional linear systems and we have carried a thorough analysis of the effects of the model parameters in shaping the impedance and phase profiles. This dependence is complex and involves changes in the response attributes in ways that are not always intuitive. For instance, an increase in the resonant frequency may be accompanied by a decrease in the natural frequency, changes in both the resonant and natural frequencies may be accompanied by constancy of the phasonant frequency, and an increase in the time-scale separation between the participating variables leads not only to a decrease in the resonant and phasonant frequencies but also
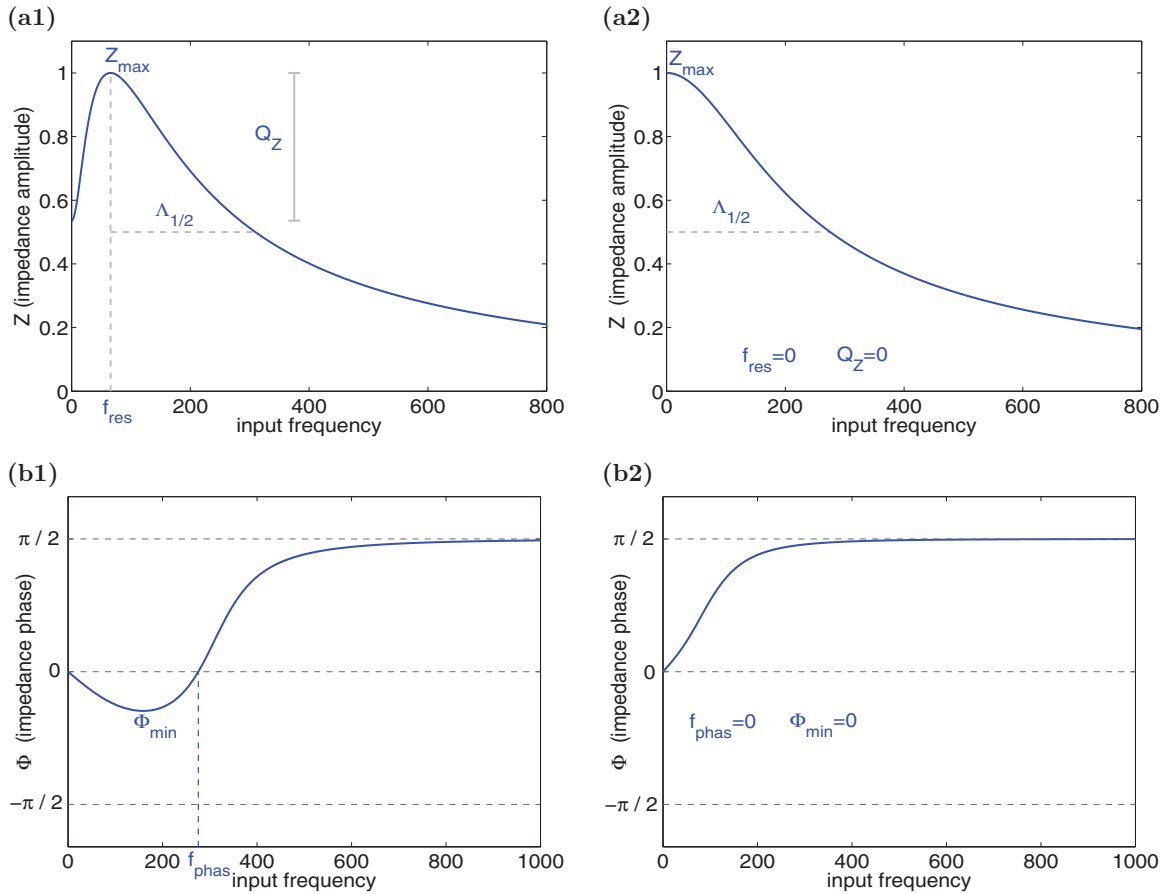
FIG. 1. (Color online) Schematic diagrams of the impedance (a) and phase (b) profiles (impedance and phase as a function of the input frequency f). (a1) Band-pass filter (resonance). (a2) Low-pass filter (no resonance). (b1) Zero-frequency crossing (phasonance). (b2) Monotonically increasing and positive phase (no phasonance). (a) The resonant frequency f_{res} is the input frequency f at which the impedance $Z(f)$ reaches its maximum Z_{max}. The resonance amplitude $Q_Z = Z_{max} - Z(0)$ measures the resonance power. The half-width frequency band $\Lambda_{1/2}$ is the length of the frequency interval in between f_{res} and the input frequency value at which $Z(f) = Z_{max}/2$. It measures the system's selectivity to incoming frequencies close to f_{res}. (b) The phasonant frequency f_{phas} is the zero-crossing phase frequency. The minimum phase ϕ_{min} measures the magnitude of the negative phase.

to an amplification of the response (increase of the maximal impedance and resonant amplitude).

In this paper, we use a method developed in Ref. [15] to investigate the linear mechanisms of generation of resonance and phasonance in the EC cell model as the result of increases in the double layer capacitance and the baseline (constant) applied potential and to track the changes in the attributes of the impedance and phase profiles as these parameters vary. We focus on parameter regimes for which the underlying linearized system has either a stable node or a stable focus and away from the existence of limit cycles for the unforced system.

EC cells as well as other excitable systems such as chemical reactions far from equilibrium share many dynamic properties with neuronal systems. They can signal either as the result of brief perturbation pulses or display sustained oscillations [1,2,9,19,20]. Oscillatory behavior is ubiquitous in the nervous system and has been implicated in cognition and motor behavior [21–24] in both health and disease [25]. It has been proposed that the electrochemical interface my serve as a simplified model for the understanding of neural network dynamics [11]. Since many neuron types exhibit

resonance [26], which is believed to play a significant role in the generation of neuronal oscillations, it is key to understand both the resonant properties of EC cells and their similarities and differences with the resonant properties of neurons as a way to understanding the computational properties of EC cells and, potentially, networks consisting of EC cells.

We note that the concept of resonance we use in this study [26] differs from studies on stochastic resonance [18], where the signals are amplified by optimal noise levels rather than oscillatory input frequencies.

II. METHODS

A. Phenomenological EC-cell model

We consider the following phenomenological model introduced in Ref. [17]. The conservation of charge equation is given by

$$\epsilon \dot{v} = \frac{q - v}{R} - w p(v) + I_{in}(t), \tag{1}$$

where v is the electric potential, w the surface concentration, ϵ is the double layer capacitance, R is the ohmic resistance, q

is the (baseline) applied potential, $I_{in}(t)$ is the external applied current, and

$$p(v) = a_1 v + a_2 v^2 + a_3 v^3. \tag{2}$$

The left-hand side in Eq. (1) represents the current flowing through the double layer capacitance, the first and second terms in the right hand side of Eq. (1) represent the total current flowing through the system and the faradaic current due to the electrochemical reaction, respectively. We use the same values of a_1, a_2, and a_3 as in Refs. [17,18]. The surface concentration obeys the following mass balance equation:

$$\dot{w} = -\frac{q-v}{R} + 1 - w + \alpha w p(v). \tag{3}$$

The first and second terms term in the right-hand side represent diffusion and migration due to potential gradients, respectively.

For external sinusoidal inputs we use the following notation:

$$I_{in}(t) = A_{in}\sin(\Omega t) \quad \text{with} \quad \Omega = \frac{2\pi f}{T}, \tag{4}$$

where $T = 1000$ ms and $[f] =$ Hz. While for EC cells under potentiostatic control the observable is the anodic current $(q-v)/R$, in this work we consider the effects of an input current and we present our results in terms of the voltage response v. We note that the addition of a current rather than a potential input does not describe either a potentiostatically or galvanostatically controlled system, thus not allowing for a direct comparison with experiments. However, the simplified approach we use in this paper provides an insight into the resonance phenomenon in electrochemical systems that can be then adapted to more realistic situations.

We rescale time by defining

$$t = \frac{\hat{t}}{\epsilon}. \tag{5}$$

Substitution into (1)–(3) yields

$$v' = \frac{q-v}{R} - wp(v) + I_{in}(t) \tag{6}$$

and

$$w' = \epsilon\left[-\frac{q-v}{R} + 1 - w + \alpha w p(v)\right], \tag{7}$$

where the "prime" sign denotes derivative with respect to the new time $\hat{t}$ and we have dropped the "hat" sign from both $\hat{t}$ and

$$\hat{I}_{in}(\hat{t}) = I_{in}(\hat{t}/\epsilon). $$

B. Linearized model

We linearize the autonomous part of Eqs. (1)–(3) around a fixed point $(\bar{v},\bar{w})$ by defining

$$x = v - \bar{v}, \quad y = w - \bar{w}. \tag{8}$$

The linearized equations are

$$x' = -ax - by \tag{9}$$

and

$$y' = cx - dy, \tag{10}$$

where

$$a = \frac{1}{R} + \bar{w}p'(\bar{v}), \quad b = p(\bar{v}),$$

$$c = \epsilon\left(\frac{1}{R} + \alpha\bar{w}p'(\bar{v})\right), \quad d = \epsilon(1 - \alpha p(\bar{v})). \tag{11}$$

The number of parameters in system (9) and (10) can be reduced by an additional rescaling,

$$x = v - \bar{v}, \quad y = (w - \bar{w})\frac{d}{c}, \quad \bar{t} = dt. \tag{12}$$

The reduced linearized equations are given by

$$x' = -\gamma_1 x - \gamma_2 y \tag{13}$$

and

$$y' = x - y, \tag{14}$$

where

$$\gamma_1 = \frac{a}{d} = \frac{1 + R\bar{w}p'(\bar{v})}{\epsilon R(1 - \alpha p(\bar{v}))},$$

$$\gamma_2 = \frac{bc}{d^2} = p(\bar{v})\frac{1 + R\alpha\bar{w}p'(\bar{v})}{\epsilon R(1 - \alpha p(\bar{v}))^2}. \tag{15}$$

C. Impedance and impedance-like functions

The response (after transients have disappeared) of a linear system such as (13) and (14) receiving sinusoidal current inputs of the form (4) in the first equation is given by

$$x_{out}(t;f) = A_{out}(f)\sin(\Omega t + \phi(f)) \tag{16}$$

where $\phi(f)$ is the phase shift (or phase) defined as the difference between the peaks of the input $I_{in}(t;f)$ and the output $x_{out}(t;f)$ and Ω is given by (4).

Linear systems exhibit resonance if there is a peak in the amplitude of the impedance function $Z(f)$ given by

$$|Z(f)| = \frac{A_{out}(f)}{A_{in}} \tag{17}$$

at some positive (resonant) frequency, f_{res}. As mentioned above, in what follows we will refer to impedance amplitude simply as the impedance $Z(f)$. In Fig. 1(a) we show representative graphs of the impedance function $Z(f)$ for a model that does [Fig. (a1)] and does not [Fig. 1(a2)] exhibit resonance. We characterize the impedance profiles using four parameters: (i) f_{res}, (ii) the maximum impedance $Z_{max} = Z(f_{res})$, (iii) the resonance amplitude $Q_Z = Z_{max} - Z(0)$, and (iv) the half-width frequency band $\Lambda_{1/2}$ defined as the frequency interval in between f_{res} and the input frequency value at which $Z(f) = Z_{max}/2$ that measures the frequency selectivity. Linear systems have a higher selectivity to inputs with frequencies around f_{res} the narrower the graph of $Z(f)$. In Fig. 1(b) we show two representative graphs of the phase $\phi(f)$ where ϕ vanishes at a nonzero value of f [Fig. 1(b1)] and ϕ is always positive [Fig. 1(b2)]. We refer to the ability of the system to exhibit a zero-phase frequency response at a nonzero frequency as *phasonance* and to the corresponding frequency

as the *phasonant* frequency f_{phas}. In Fig. 1(b1), $f_{phas} > 0$. The voltage response is "advanced" and "delayed" with respect to the peak of the input current for lower and higher frequency inputs respectively. Although phase-advance and phase-delay are ambiguous concepts to describe phase differences between inputs and outputs in oscillatory systems, we use them since typical phase differences lie in the range $(-\pi/2, \pi/2)$. In Fig. 1(b2), $f_{phas} = 0$, that is, the voltage response is delayed for all values of f. We characterize the phase profiles using two attributes: (i) f_{phas} and (ii) the minimum phase ϕ_{min}.

III. RESULTS

A. Stability and resonant properties of two-dimensional linear systems revisited

In Ref. [15], we have conducted a through analysis of the stability and resonant properties of two-dimensional linear systems of the form (13) and (14), and we have identified three primary mechanisms of generation of resonance. Here we briefly review some of these results for future use. We refer the reader to Ref. [15] for more details.

Figure 2 shows the superimposed stability and resonance diagrams in γ_1-γ_2 parameter space. The blue curves separate between regions having different stability properties. In the stable foci region, the natural frequency f_{nat} increases across level sets parallel to the curve separating stable foci from stable nodes [Fig. 3(a)]. The red curve separates between regions in parameter space for which the system does (above) and does not (below) exhibit resonance. Figure 2 demonstrates that resonance and intrinsic (damped) oscillations may occur in the absence of each other. In particular, for large enough values of γ_1, the system may exhibit resonance without intrinsic (damped) oscillations.

We focus on regions in parameter space for which the fixed point (focus or node) is stable. Within this region, the resonant frequency f_{res} increases across level sets parallel to the resonance curve [Fig. 3(b)]. The qualitatively different ways in which f_{res} and f_{nat} change in γ_1-γ_2 parameter space demonstrates that intrinsic oscillations and resonance are different phenomena governed by different mechanisms.

Specifically, as γ_2 increases for fixed values of γ_1, both f_{res} and f_{nat} are either zero or monotonically increasing. However, as γ_1 increases for fixed values of γ_2, f_{res} is always increasing, while f_{nat} first increases and then decreases. In contrast to f_{res} and f_{nat} that change with both γ_1 and γ_2, f_{phas} increases with γ_2 but is independent on γ_1 [Fig. 3(c)].

For a low-pass filter, $Z_{max} = Z(0)$ [Fig. 1(a2)]. Resonance requires that the resonance amplitude $Q_Z = Z_{max} - Z(0) > 0$. The two quantities Z_{max} and $Z(0)$ follow different patterns as the change in γ_1-γ_2 parameter space, as reflected in the nonconstant values of Q_Z in Fig. 3(d). The values of Z_{max} and $Z(0)$ are larger for the lower values of γ_1 [15]. In particular, Z_{max} is significantly larger for negative than for positive values of γ_1. Both quantities decrease as γ_1 and γ_2 increase [15].

Changes in γ_1 and γ_2 span trajectories in parameter space. Resonance is generated as these trajectories cross the resonance curve in Fig. 2. For the linear system (13) and (14), there are two possible types of trajectories as each one of γ_1 and γ_2 change, spanning horizontal and vertical lines respectively. This gives rise to two of the primary linear mechanisms of generation of resonance described below. The third linear mechanism of generation of resonance involves changes in the time scale separation (ϵ) between the variables v and w and is not apparent from the form of the reduced (rescaled) linear system (13) and (14) but requires a closer inspection of the definitions of these parameters. From (15), changes in ϵ span oblique lines in γ_1-γ_2 parameter space, which approach zero as $\epsilon \to \infty$. Additional, nonlinear trajectories in parameter space can be generated as the EC cell model parameters change.

Linear trajectories (vertical, horizontal, and oblique) in γ_1-γ_2 parameter space are spanned by generic linear systems, while nonlinear trajectories require an *a priori* knowledge of the physical system under consideration. The resonant properties for generic linear systems are discussed below in this section. The resonant properties of the EC model along nonlinear trajectories will be discussed in Sec. III C.

The first two primary linear mechanisms of generation of resonance involve unbalanced changes in Z_{max} and $Z(0)$, leading to changes in Q_Z [Fig. 3(d)]. In the first case, both decrease as γ_2 increases, but $Z(0)$ decreases faster than Z_{max}, thus increasing Q_Z above zero. In the second case, both
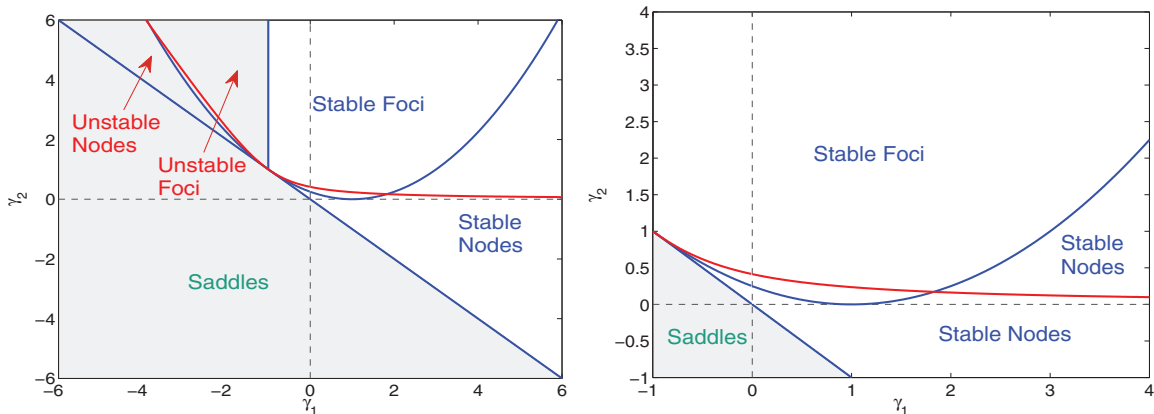
FIG. 2. (Color online) Superimposed stability and resonance diagrams for the reduced two-dimensional linear system (13) and (14) in γ_1-γ_2 parameter space. The blue curves separate between regions with different stability properties. The red curve separate between regions where the system does (above) and does not (below) exhibit resonance. Intrinsic oscillations and resonance may occur in the absence of the other. The right panel is a magnification of the left one.
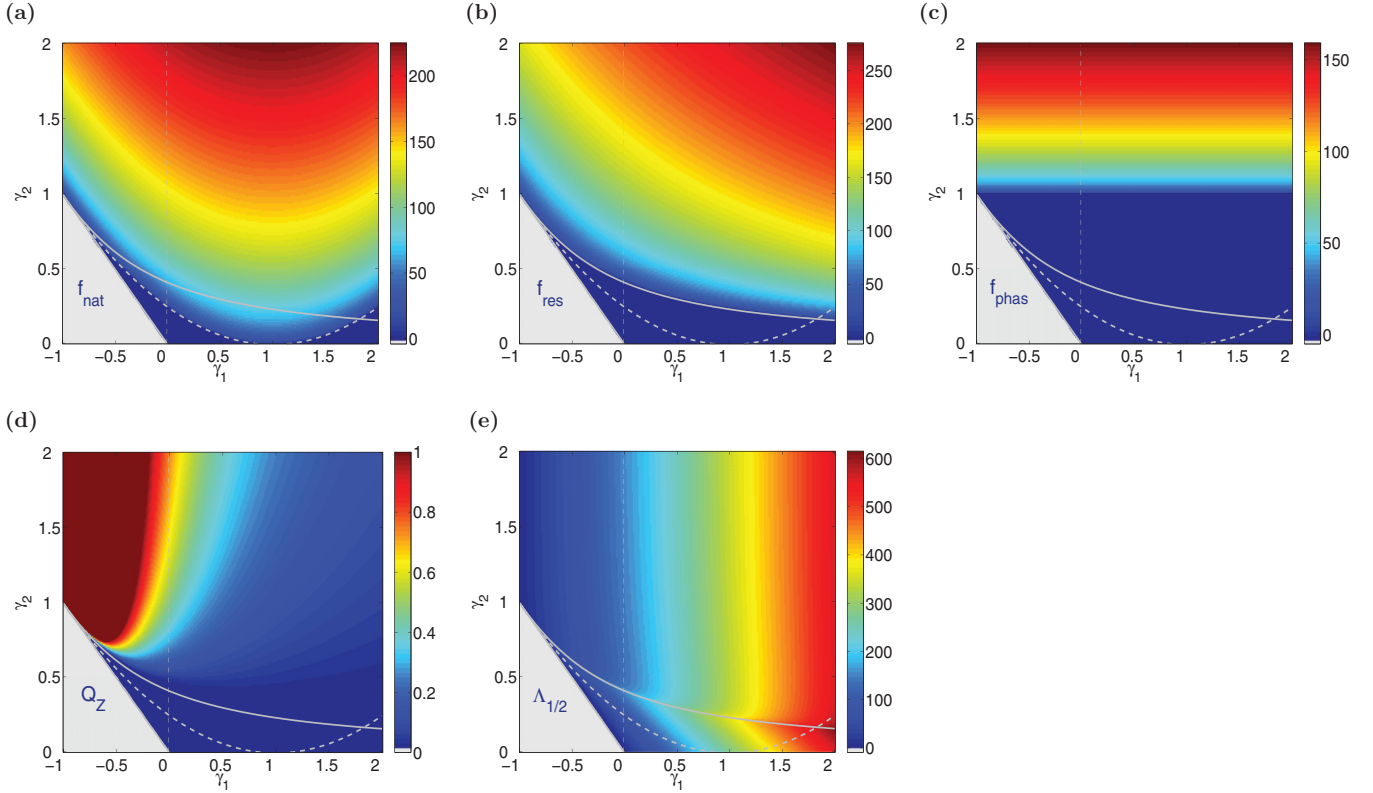
FIG. 3. (Color online) Representative attributes of the impedance and phase profiles in γ_1-γ_2 parameter space for the linear system (13) and (14) . Colorbar: Values of the corresponding attribute. (a) Natural frequency f_{nat}. (b) Resonant frequency f_{res}. (c) Phasonant frequency f_{phas}. (d) Resonance amplitude Q_Z. The red region corresponds to $Q_Z \geqslant 1$. The value of Q_Z dramatically increases in this region from right to left, and it was set equal to 1 for the graph to capture the whole range of values of Q_Z. (e) Half-bandwidth $\Lambda_{1/2}$. The system's selectivity increases as $\Lambda_{1/2}$ decreases.

quantities increase as γ_1 decreases, but Z_{max} increases faster than $Z(0)$, thus increasing Q_Z.

The third mechanism of generation of resonance involves changes along the oblique lines parametrized by ϵ. As ϵ decreases, these ϵ lines cross the resonance (red) curve in Fig. 2. From (A8) (in Appendix), $Z(0)$ is independent of ϵ, so this mechanisms involves only changes in Z_{max}. The direction of motion of the ϵ lines determines the level of amplification of the EC cell's response, which is more pronounced for negative slopes than for positive ones.

The fidelity of the EC cell's response to oscillatory inputs depends not only on Z_{max} and Q_Z but also on the half-bandwidth $\Lambda_{1/2}$ [Fig. 3(e)], which increases with γ_1, making the cell more selective, and is almost constant in the γ_2 direction.

The qualitatively different ways in which the impedance attributes (f_{res}, f_{phas}, Z_{max}, Q_Z, and $\Lambda_{1/2}$) change with both γ_1 and γ_2 demonstrates the complexity of the resonance phenomenon [15] and suggest that an optimal response over all attributes is difficult to achieve except in some restricted parameter regimes.

B. Dynamics of the autonomous EC cell model

Here we use numerical simulations and phase-plane analysis to investigate the dynamics of the autonomous EC cell. Our goal is to establish the parameter sets for which the

model exhibits stable nodes and foci and to examine the types of nonlinearities present in the model and how their variation depends on the model parameters. We first consider the effects of changes in q for fixed values of α, ϵ, and R. We focus on two parameter sets that have qualitatively different phase-plane diagrams. One of these has been previously used in Refs. [17,18] in a different context. Finally, for future use, we investigate the effects of changes in α and R for fixed values of the remaining parameters.

1. Effects of changes in q

Figure 4 shows the phase plane and voltage traces for representative values of q and $\alpha = 0.1$, $\epsilon = 0.03$, and $R = 10$. Changes in q affect the shape of both the v and w nullclines [red and green curves in the (a) panels] in qualitatively different ways. As q increases the v nullcline develops cubic-type nonlinearities that are more pronounced for the larger values of q. The w nullcline, instead, remains quasilinear as q increases, but it is translated in almost parallel directions towards larger values of v. For low-enough values of q, the system has a stable node [Fig. 4(a1)] and the dynamics is quasilinear. As q increases, the fixed-point transitions to a stable focus [Fig. 4(a2)]. As q increases further, the system undergoes a supercritical Hopf bifurcation. The fixed point becomes unstable and a stable limit cycle is created [Fig. 4(a3)]. Its amplitude increases with q as the cubic
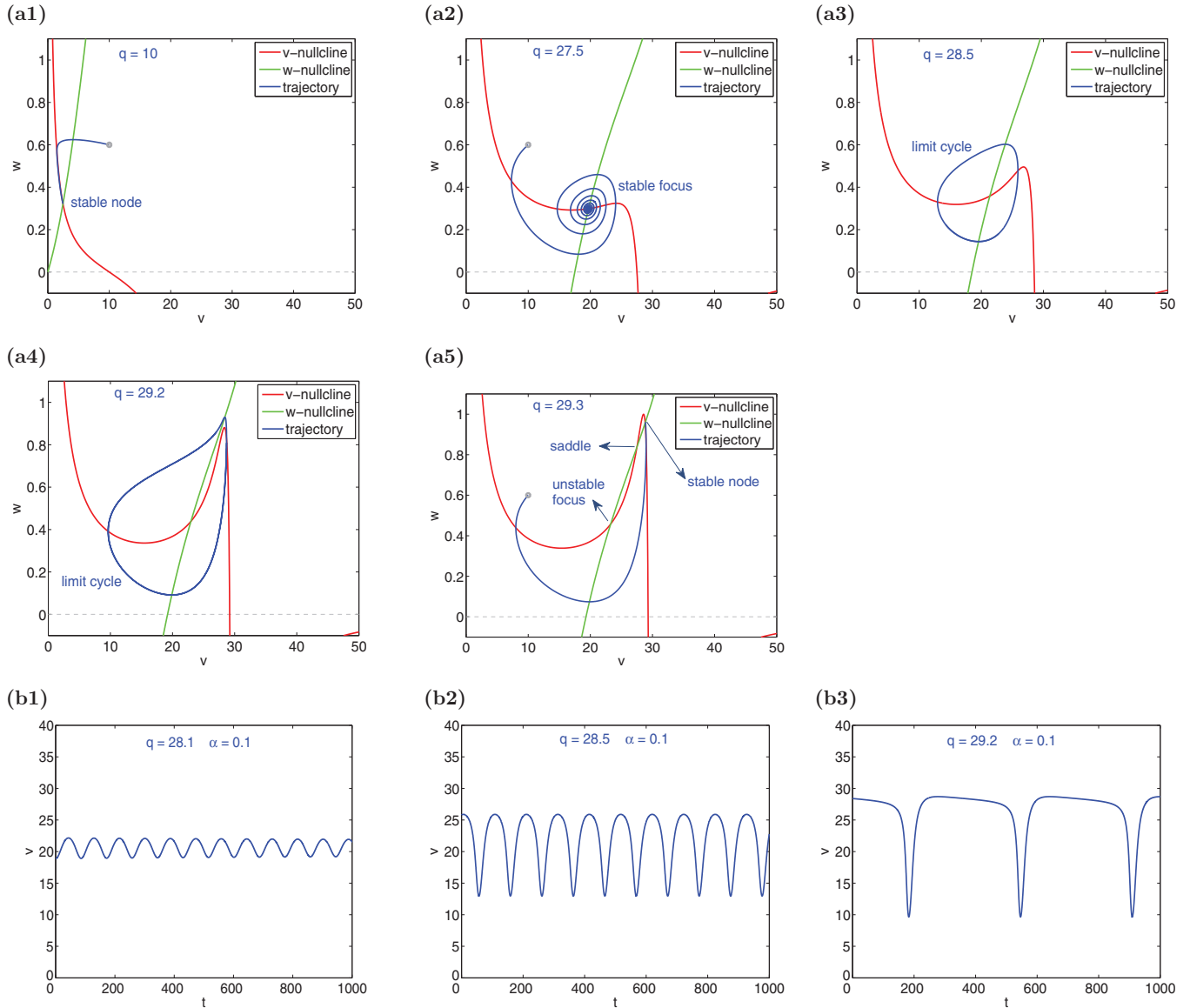
FIG. 4. (Color online) Dynamics of the EC cell model (6) and (7) for representative values of q and $\epsilon = 0.03$, $R = 10$, and $\alpha = 0.1$. (a) Phase-plane diagrams for representative values of q: (a1) $q = 10$, (a2) $q = 27.5$, (a3) $q = 28.5$, (a4) $q = 29.2$, and (a5) $q = 29.3$. Fixed points are located in the intersection of the v and w nullclines. Each panel shows a representative trajectory initially at the gray dot, either converging to the stable fixed point [panels (a1), (a2), and (a5)] or displaying limit-cycle oscillations [panels (a3) and (a4)]. As q increases, the limit cycle is created in a supercritical Hopf bifurcation and it disappears in a saddle node in an invariant circle (SNIC) bifurcation. (b) Voltage traces for representative values of q in the limit cycle regime: (b1) $q = 28.1$, (b2) $q = 28.5$, and (b3) $q = 29.2$.

nonlinearity becomes more pronounced [Fig. 4(a4)]. The limit cycle oscillations are terminated at a saddle node in an invariant circle (SNIC) bifurcation as the two nullclines intersect [Fig. 4(a5)]. Figure 4(b) illustrates the representative voltage traces for the limit cycle oscillations. As q increases the amplitude increases and the frequency decreases.

In Fig. 5, $\alpha = 0.5$, $\epsilon = 0.03$, and $R = 10$. The differences in the values of α between this figure and Fig. 4, are correlated with qualitative differences in the properties of the w nullcline: (i) it has a negative slope for $\alpha = 0.5$ [Fig. 5(a1)], while it has a positive slope for $\alpha = 0.1$ [Fig. 4(a1)], and (ii) for $\alpha = 0.5$, a second branch of the w nullcline emerges for large enough values of q [Fig. 5(a3)] and it shifts down as q increases, in addition to the translation as discussed above for $\alpha = 0.1$. The limit

cycle oscillations are terminated when the v nullcline intersects this additional branch and the system undergoes a SNIC bifurcation [Fig. 5(a5)]. While the sequence of voltage patterns is similar, the qualitative differences between the two cases is expected to affect the responses of cells to oscillatory inputs.

2. Effects of changes in α

Comparison between the voltage traces for $\alpha = 0.1$ [Fig. 5(b1)] and $\alpha = 0.5$ (Fig. 4(b1)) demonstrates that as α increases, the amplitude of the limit cycle oscillations increases and the frequency slightly increases.

In Fig. 6 we present the phase-plane diagrams for various representative values of α and fixed values of $\epsilon = 0.3$, $R =$
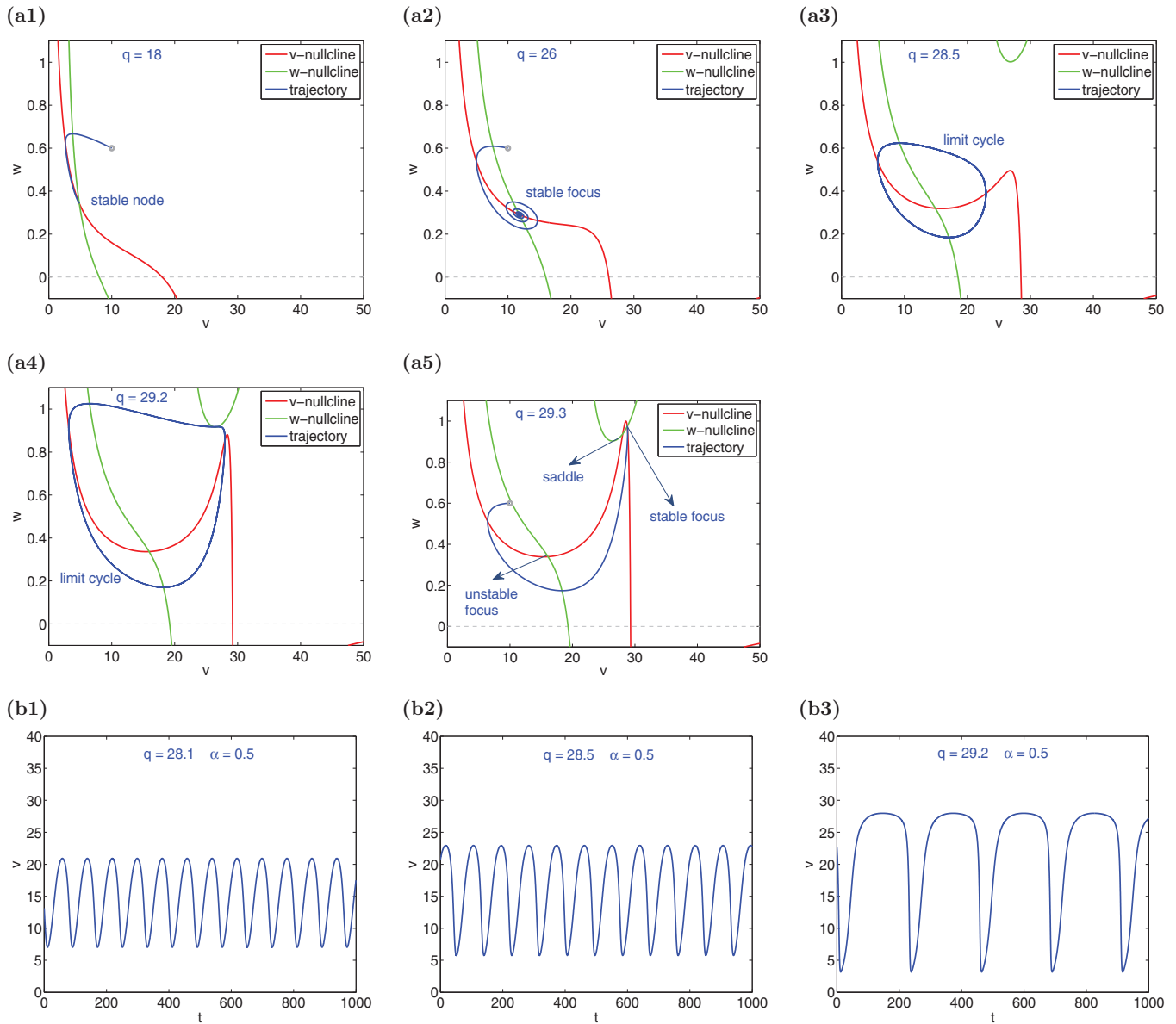
FIG. 5. (Color online) Dynamics of the EC cell model (6) and (7) for representative values of q and $\epsilon = 0.03$, $R = 10$, and $\alpha = 0.5$. (a) Phase-plane diagrams for representative values of q: (a1) $q = 18$, (a2) $q = 26$, (a3) $q = 28.5$, (a4) $q = 29.2$, and (a5) $q = 29.3$. Fixed points are located in the intersection of the v and w nullclines. Each panel shows a representative trajectory initially at the gray dot, either converging to the stable fixed point [panels (a1), (a2), and (a5)] or displaying limit-cycle oscillations [panels (a3) and (a4)]. As q increases, the limit cycle is created in a supercritical Hopf bifurcation and it disappears in a saddle node in an invariant circle (SNIC) bifurcation. (b) Voltage traces for representative values of q in the limit cycle regime: (b1) $q = 28.1$, (b2) $q = 28.5$, and (b3) $q = 29.2$.

10, and $q = 28.5$. For these parameter values, the EC system displays limit cycle oscillations for both $\alpha = 0.1$ [Fig. 4(a3)] and $\alpha = 0.5$ [Fig. 5(a3)]. Changes in α affect only the shape of the w nullcline. We note that a negative value of α, as in Fig. 6(e), may have no physical meaning. However, we include this example in our study to provide a more general picture of the EC dynamics and to illustrate the presence of a transition from a stable limit cycle [Fig. 6(d)] to a stable focus [Fig. 6(e)] as the value of α decreases. Similar phase planes may exist for positive values of α. As α increases, the limit cycle oscillations are both created and terminated in supercritical Hopf bifurcations. Note that the change in sign

for the slope of the w nullcline discussed above occurs in between Figs. 6(c) and 6(d).

3. Effects of changes in R

Figure 7 shows the phase planes and voltage traces for representative values of R and $\alpha = 0.1$, $\epsilon = 0.03$, and $q = 28.5$. Changes in R affect the shapes of both the v and w nullclines. For large values of R, the dynamics is quasilinear and the fixed points are stable nodes [Fig. 7(a1)]. As R decreases the cubic nonlinearity in the v nullcline becomes more pronounced and the fixed-point transitions from a stable node to a stable focus. As R decreases further, a stable
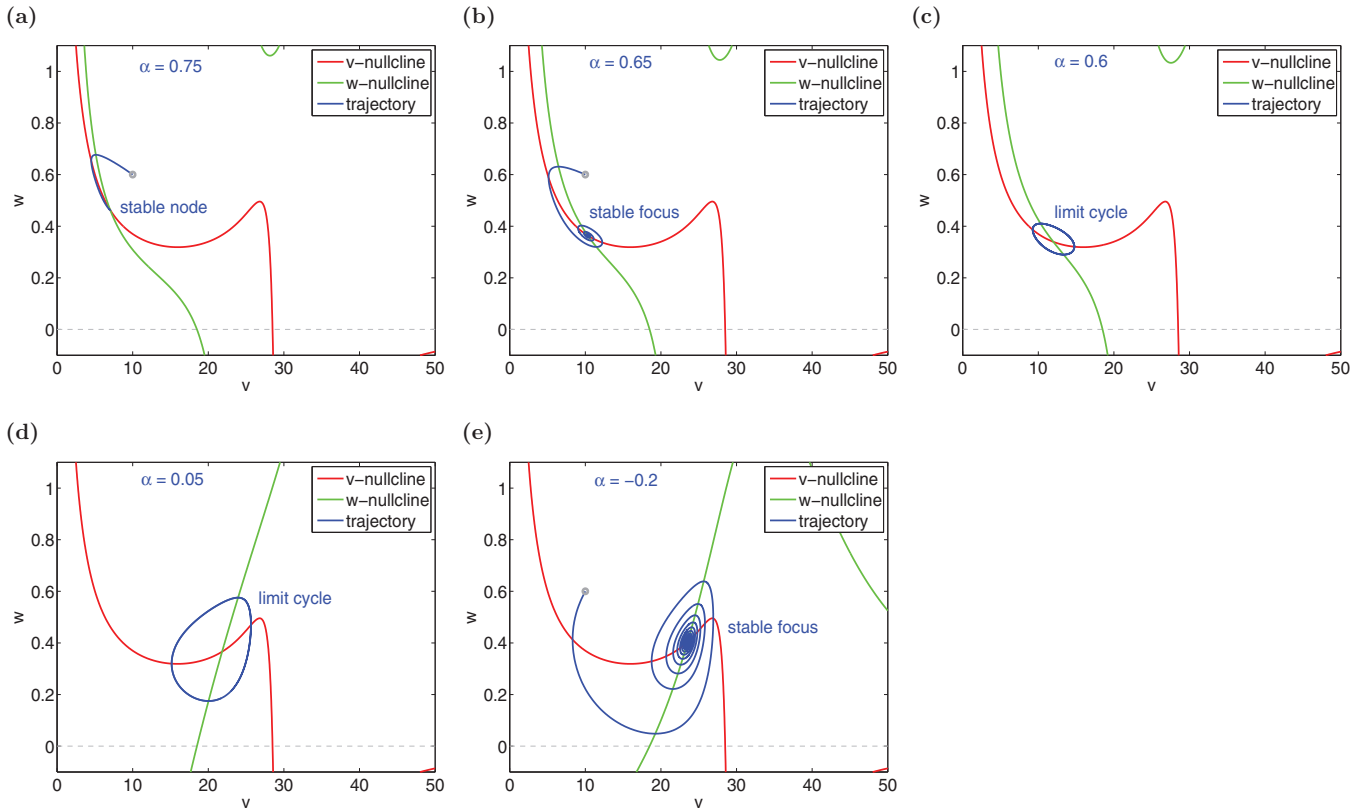
FIG. 6. (Color online) Phase plane for system (6) and (7) for representative values of α and $\epsilon = 0.03$, $R = 10$, and $q = 28.5$. Fixed points are located in the intersection of the v and w nullclines. Each panel shows a representative trajectory initially at the gray dot, either converging to the stable fixed point [panels (a), (b), and (e)] or displaying limit-cycle oscillations [panels (c) and (d)]. As q increases, the limit cycle is both created and terminated in a supercritical Hopf bifurcation. (a) $\alpha = 0.75$, (b) $\alpha = 0.65$, (c) $\alpha = 0.6$, (d) $\alpha = 0.05$, and (e) $\alpha = -0.2$.

limit cycle is created in a supercritical Hopf bifurcation, and terminated in an additional Hopf bifurcation for an even lower values of R. As expected, the amplitude of the limit cycles is larger for intermediate values of R away from the Hopf bifurcation points [Fig. 7(b)].

C. Resonance and phasonance in the linearized EC-cell model

We now investigate the linear resonant properties of the EC cell model (6) and (7). The linearized EC cell model is given by Eqs. (13) and (14) with γ_1 and γ_2 given by (15). We focus on the linear mechanisms of generation of resonance and phasonance and the effects of the physicochemical parameters (q, ϵ, R, and α) on the attributes of the impedance and phase profiles. We limit our discussion to parameter values yielding stable fixed points (foci and node) and leave out the parameter regimes corresponding to limit cycle oscillations, which are beyond the scope of this paper.

Our discussion in Sec. III A (see also Ref. [15]) provides an insight into the mechanisms of generation of resonance and phasonance in generic linear systems of the form (13) and (14) but not into the mechanisms of generation of these phenomena in the linearized EC cell model. As is clear from the nullcline nonlinearities in the phase-plane diagrams presented in Sec. III B and from Eqs. (15), changes in the physicochemical parameters generate nonlinear trajectories in γ_1-γ_2 parameter space rather than horizontal and vertical trajectories generated by changes in the linearized coefficients (γ_1 and γ_2). We

emphasize that the contribution of the the physicochemical parameters to the linearized coefficients in Eqs. (15) is not only explicit but also implicit through the values of the fixed point $(\bar{v}, \bar{w})$, a fact that is sometimes overlooked.

We use a technique developed in Ref. [15], which consists on plotting the trajectories parametrized by q (or any other parameter under consideration) superimposed on the stability/resonant diagrams in the γ_1-γ_2 parameter space presented in Fig. 1. These diagrams can be used in conjunction with Fig. 3 to learn how the various impedance and phase attributes change with the EC cell model parameters. The resulting diagrams together with representative examples of the impedance and phase profiles are presented in Figs. 8–13.

1. Effect of changes in q and ϵ

In Fig. 8 we present representative trajectories in γ_1-γ_2 parameter space parametrized by q for three representative values of ϵ. The right panel in Fig. 8 is an expansion of the left one to capture a larger region in parameter space. Trajectories are initially located in a close vicinity of the resonant (red) curve and terminate either at a supercritical Hopf bifurcation ($\epsilon = 0.03$), as they cross the vertical line $\gamma_1 = -1$ (separating between stable and unstable foci) or at a saddle-node bifurcation ($\epsilon = 0.1$ and $\epsilon = 0.2$). For a significant range of values of q, the EC cell exhibits resonance in the absence of damped or sustained oscillations. These range of values of q is larger the smaller ϵ.
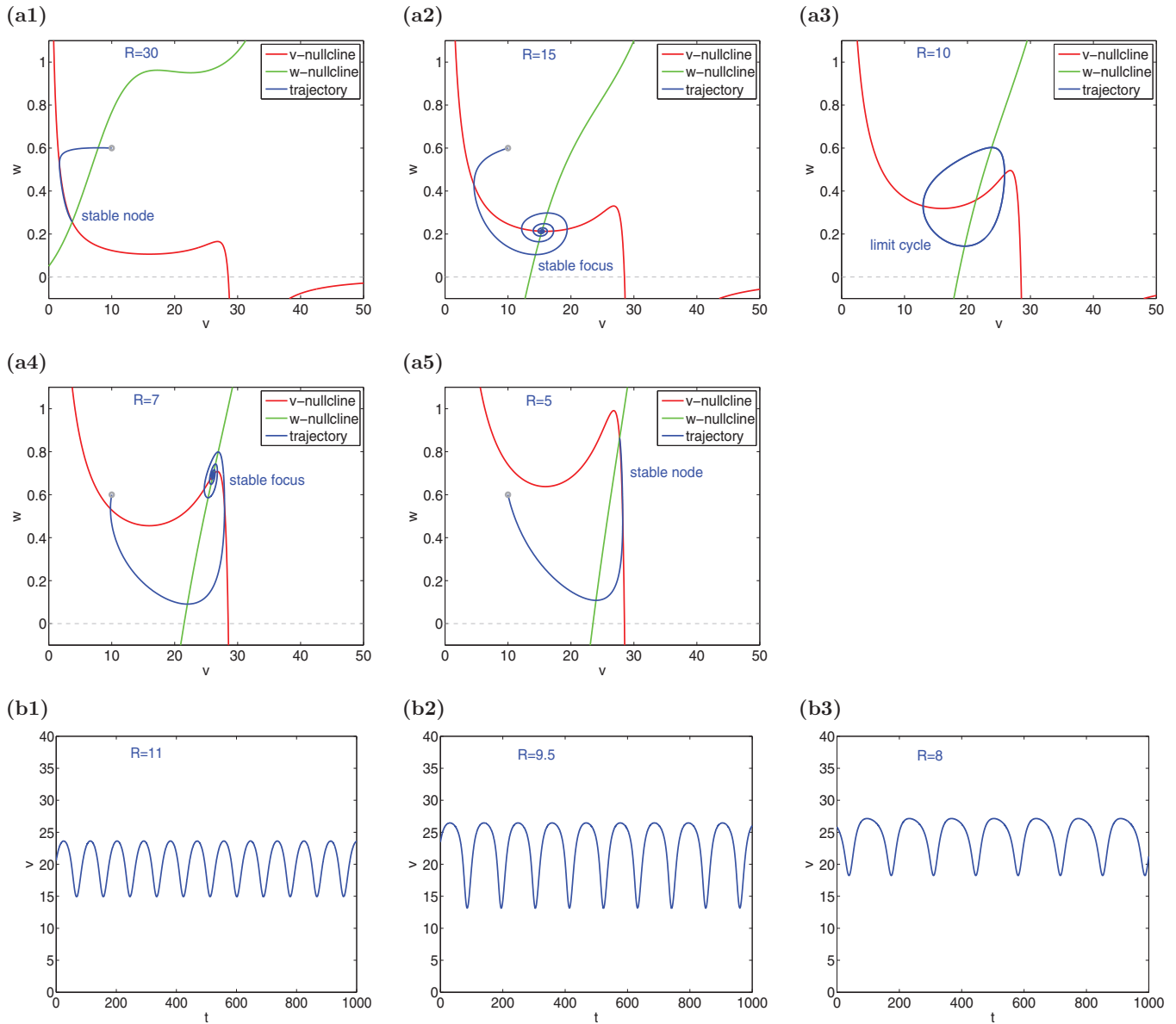
FIG. 7. (Color online) Dynamics of the EC cell model (6) and (7) for representative values of R and $\epsilon = 0.03$, $q = 28.5$, and $\alpha = 0.1$. (a) Phase-plane diagrams for representative values of q: (a1) $R = 30$, (a2) $R = 15$, (a3) $R = 10$, (a4) $R = 7$, and (a5) $R = 5$. Fixed points are located in the intersection of the v and w nullclines. Each panel shows a representative trajectory initially at the gray dot, either converging to the stable fixed point [panels (a1), (a2), and (a5)] or displaying limit-cycle oscillations [panels (a3) and (a4)]. As R increases, the limit cycle is created and terminated in supercritical Hopf bifurcations. (b) Voltage traces for representative values of R in the limit cycle regime: (b1) $R = 11$, (b2) $R = 9.5$, and (b3) $R = 8$.

Comparison between Figs. 8 and 3 shows that the attributes of the impedance and phase profile behave differently as q changes during the ascending (I) and descending (II) portions of the trajectories. We present representative examples for $\epsilon = 0.03$ in Fig. 9. Figures 9(a) and 9(b) correspond to the ascending and descending portions of the trajectory, respectively. The values of q in Fig. 9 are marked with a black dot in the corresponding trajectory ($\epsilon = 0.03$) in Fig. 8.

As q increases along the ascending portion of the trajectory, $f_{\rm res}$ increases and the response becomes more amplified due to the increase in both $Z_{\rm max}$ and Q_Z [Fig. 9(a)]. In addition, the response becomes more selective ($\Lambda_{1/2}$ decreases). The amplification of the response when q increases along the

descending (II) portion of the trajectory is more pronounced than on the ascending portion (I) [Fig. 9(c)]. However, on the former $f_{\rm res}$ decreases with increasing values of ϵ rather than increase. These effects are present, but they are less pronounced for large values of ϵ (not shown).

The dependence of $f_{\rm phas}$ with q follows a similar pattern as $f_{\rm res}$ [Figs. 9(c) and 9(d)]: $f_{\rm phas}$ increases with q on the ascending portion of the trajectory (I) and decreases with q on its descending portion (II). Note that $\phi_{\rm min}$ is almost insensitive to changes in q on the descending portion [Fig. 9(d)].

This analysis demonstrates that although the EC cell response is more amplified for parameter values close to the supercritical Hopf bifurcation, or corresponding to stable
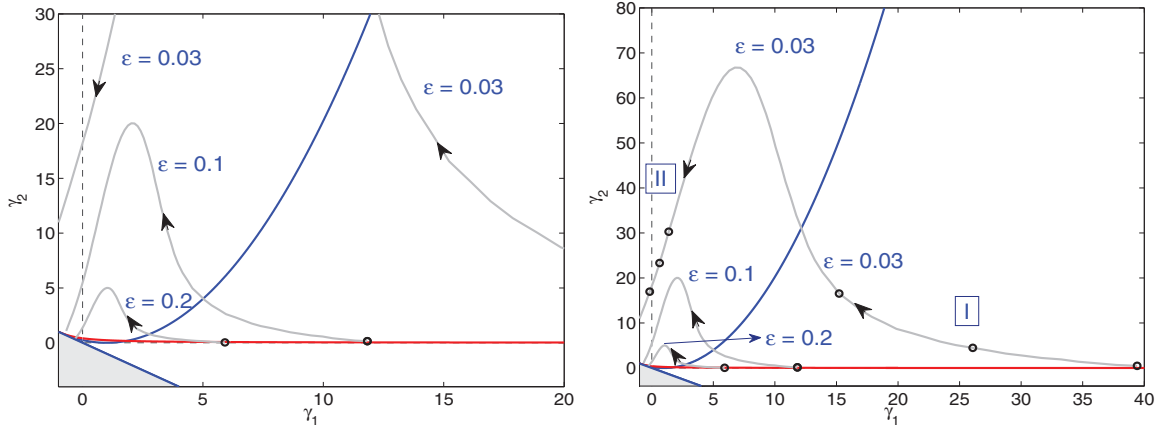
FIG. 8. (Color online) The effect of q on the EC cell linear resonance properties for representative values of ϵ. Trajectories parametrized by q superimposed on the stability/resonant diagrams in γ_1-γ_2 parameter space (arrows indicate increasing values of q). The right panel is an extension of the left one to capture a larger region in parameter space. The stability (blue) and resonant (red) curves are as in Fig. 2(c). All trajectories (gray curves) start at $q = 0.1$ (marked by a black dot on top of the red curve). Different trajectories correspond to different values of ϵ. The trajectories are computed until the fixed point $(\bar{v}, \bar{w})$ ceases to be stable either because it becomes a saddle ($\epsilon = 0.1$ and $\epsilon = 0.2$) or because it becomes an unstable focus and a limit cycle is created (supercritical Hopf bifurcation). We used the following parameters values: $\alpha = 0.1$, $R = 10$.

foci, both resonance and phasonance are present, and are non-negligible, for parameter values corresponding to a stable node for which the EC cell cannot displays intrinsic (damped) oscillations.

2. Effects of changes in q and α

In Fig. 10 we analyze the effects of changes in q for representative values of α. These trajectories are initially
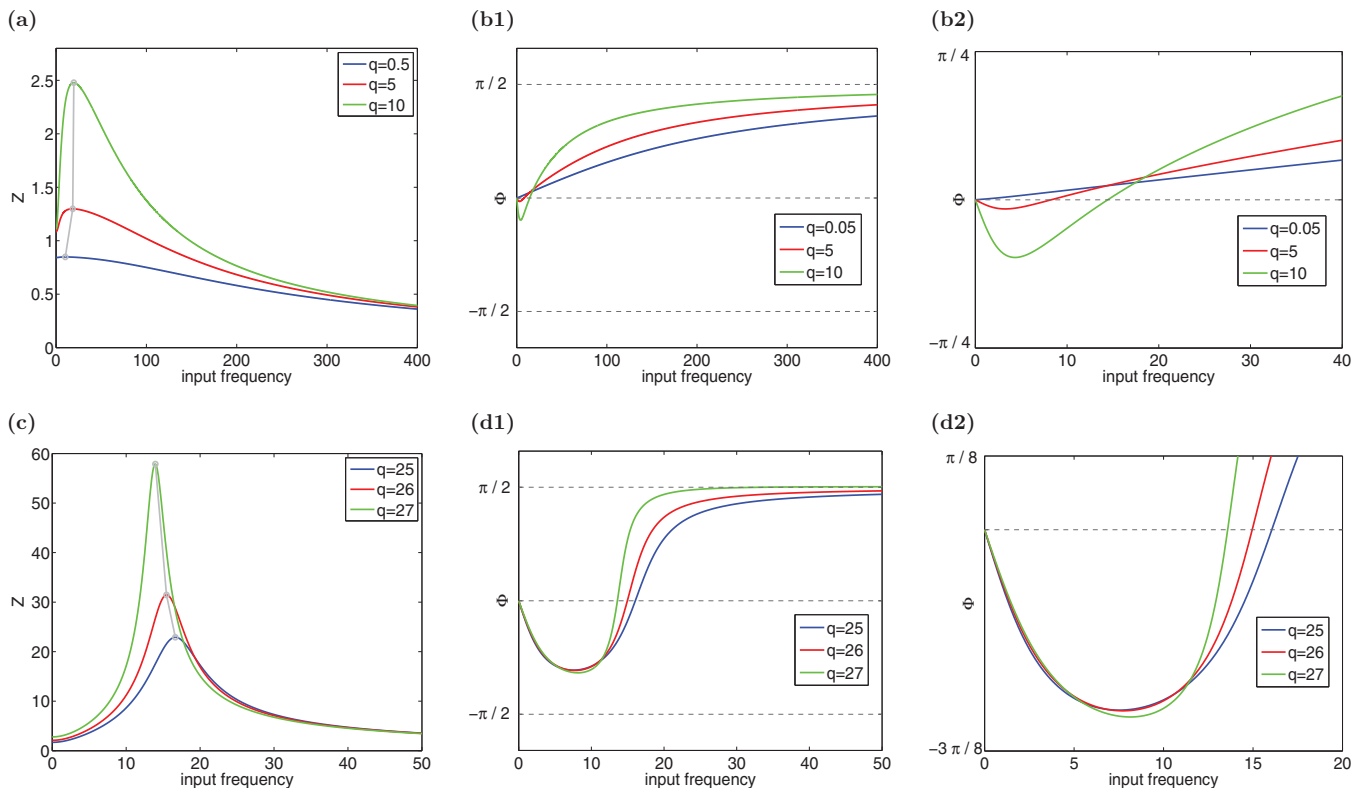
FIG. 9. (Color online) The effect of q on the resonance and phasonant properties for the linearized EC model (13) and (14) with $\epsilon = 0.03$, $\alpha = 0.1$, and $R = 10$. (a) Impedance profiles on the ascending portion (I) of the trajectories in Fig. 8. (b) Phase profiles on the ascending portion (I) of the trajectories in Fig. 8. (c) Impedance profiles on the descending (II) portion of the trajectories in Fig. 8. (d) Phase profiles on the descending (II) portion of the trajectories in Fig. 8. The values of q correspond to the black dots on the curve for $\epsilon = 0.03$ in Fig. 8. The gray curves in panels (a) and (c) join the maxima of the impedance profiles.
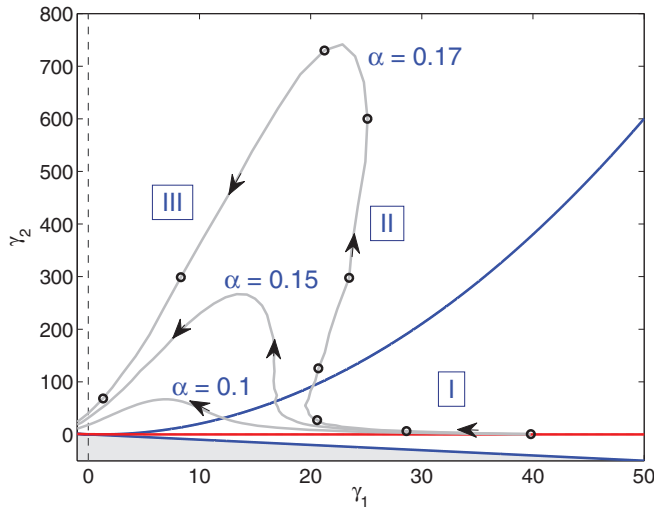
FIG. 10. (Color online) The effect of q on the EC cell linear resonance properties for representative values of α. Trajectories parametrized by q superimposed on the stability/resonant diagrams in γ_1-γ_2 parameter space (arrows indicate increasing values of q). The stability (blue) and resonant (red) curves are as in Fig. 2(c). All trajectories (gray curves) start at $q = 0.1$ (marked by the rightmost black dot on the red curve at $\gamma_2 \sim 40$). Different trajectories correspond to different values of α. The trajectories are computed until the fixed point $(\bar{v}, \bar{w})$ ceases to be stable when undergoes a supercritical Hopf bifurcation and a limit cycle is created. We used the following parameter values: $\epsilon = 0.03$, $R = 10$.

located in a vicinity of the resonance (red) curve and terminate at supercritical Hopf bifurcations as they cross the $\gamma_1 = -1$ line (separating between stable and unstable foci).

Similarly to the case discussed above, the system exhibits resonance for parameter values for which no intrinsic (damped) oscillations are possible. In contrast to the previous case, trajectories for larger values of α have three characteristic portions: an almost horizontal one (denoted by I), an ascending one (denoted by II), and a descending one (denoted by III). During the ascending phase the trajectory slightly reverses the direction of motion: The values of γ_1 on the trajectory first decrease (I), then increase (II), and finally decrease again (III).

The qualitative change in the trajectories' shape and the development of a third portion for large enough values of α is correlated with the changes observed in the phase planes where similar bifurcations occur through qualitatively different geometric mechanisms (compare Figs. 4 and 5).

The impedance and phase profiles corresponding to $\alpha = 0.17$ are presented in Fig. 11. Figures 11(a) and 11(b) correspond to the almost horizontal portion of the trajectory (I), Figs. 11(c) and 11(d) correspond to the ascending portion of the trajectory (II), and Figs. 11(e) and 11(f) correspond to the descending portion of the trajectory (III). The values of q in Fig. 11 are marked with a black dot in the trajectory for $\alpha = 0.17$ in Fig. 10.

As q increases along the almost horizontal portion of the trajectory (I), f_{res} increases, the response becomes more amplified (both Z_{max} and Q_Z increase) and more selective [Fig. 11(a)], and f_{phas} increases [Fig. 11(b)]. As q increases along the ascending portion of the trajectory (II), the trajectory becomes more amplified but both f_{res} and f_{phas} remain almost

unchanged [Figs. 11(c) and 11(d)]. As q increases along the descending portion of the trajectory (III), the response becomes more amplified, and the amplifications is more pronounced that in the previous portions, but both f_{res} and f_{phas} decrease.

In summary, although in all portions of the trajectory in parameter space the linear response of the EC cell becomes amplified and more selective as q increases, f_{res} and f_{phas} have different monotonic properties in different portions.

3. Effects of changes in R and q

In Fig. 12 we analyze the effects of changes in R for two representative values of q, $\epsilon = 0.03$ and $\alpha = 0.1$. The trajectories are initially located on the vertical line $\gamma_1 = 20$, in the stable node region, where the system exhibits resonance but not intrinsic (damped) oscillations and terminate in the same region after an excursion through the foci region. For an intermediate range of values of R, the trajectories evolve in the stable foci region. The trajectory for $q = 28.5$ crosses the vertical lines $\gamma_1 = -1$ to the unstable foci region, while for $q = 27$ the trajectory never crosses to that region and stays within the stable foci one. As discussed above, the values of R for which the trajectory is in the unstable foci region correspond to the existence of a stable limit cycle, whose study is outside the scope of this paper. The trajectories' characteristic shapes reflect the dynamics of the autonomous system as R changes (discussed in the context of Fig. 7) where stable nodes exist for both large and small values of R.

In Fig. 13 we present the impedance and phase profiles for $q = 28.5$. Figures 13(a) and 13(b) correspond to the portion marked with I, Figs. 13(c) and 13(d) correspond to the portion marked with II, and Figs. 13(e) and 13(f) correspond to the portion marked with III. As we mentioned above, we purposely leave out the parameter range corresponding to the existence of stable limit cycles.

As R increases along the portion I, there is an amplification of the response and both f_{res} and f_{phas} decrease. Consistently, with Fig. 3(e), the selectivity increases ($\Lambda_{1/2}$ decreases). In contrast, as R increases along the portion II, both f_{res} and f_{phas} increase, there is an attenuation of the response, and the selectivity decreases. The properties of the impedance and phase profiles as R increases in portion III bear similarities and differences with the two previous portions. As in portion I, f_{res} and f_{phas} decrease with increasing values of R (the change of f_{res} is very small). As in portion II, there is an attenuation of the response with increasing values of R and the selectivity decreases

IV. DISCUSSION

The response of electrochemical system to oscillatory inputs has been studied in a number of works [9–12,27–32]. In this paper we have investigated the linear mechanisms of the generation of preferred frequency responses to sinusoidal inputs in a phenomenological model of an EC cell. This model was introduced in Ref. [17] to investigate the dynamics of diffusively coupled EC oscillators and used in Ref. [18] to capture the stochastic resonant properties of EC systems. Stochastic resonance differs from the type of amplitude resonance we studied here. The former refers to the amplification of a signal
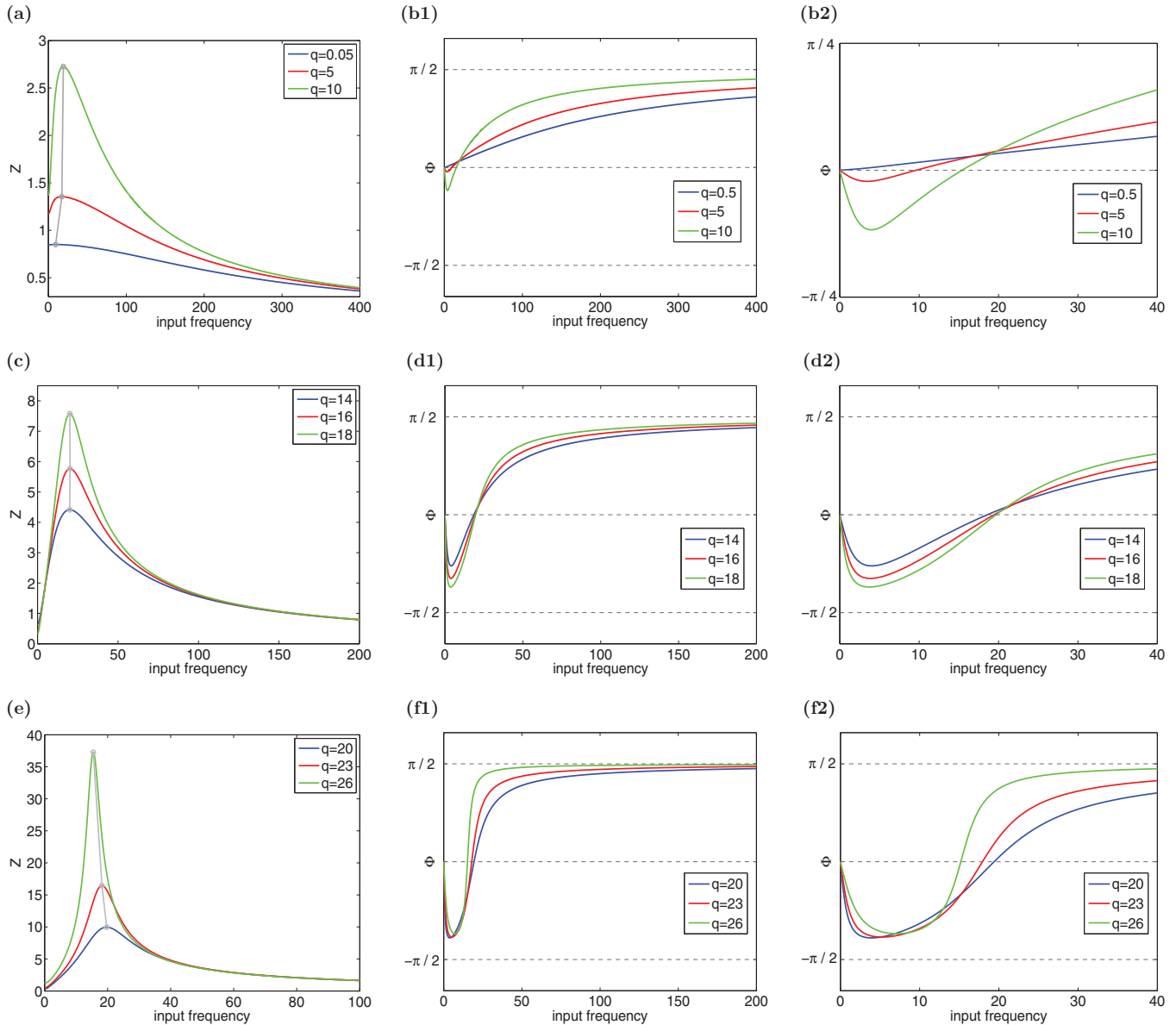
FIG. 11. (Color online) The effect of q on the resonance and phasonance properties for the linearized EC model (13) and (14) with $\epsilon = 0.03$, $\alpha = 0.17$, and $R = 10$. (a) Impedance profiles on the almost horizontal portion (I) of the trajectories in Fig. 10. (b) Phase profiles on the almost horizontal portion (I) of the trajectories in Fig. 10. (c) Impedance profiles on the ascending portion (II) of the trajectories in Fig. 10. (d) Phase profiles on the ascending portion (II) of the trajectories in Fig. 10. (e) Impedance profiles on the descending (III) portion of the trajectories in Fig. 10. (f) Phase profiles on the descending (III) portion of the trajectories in Fig. 10. The values of q correspond to the black dots on the curve for $\alpha = 0.17$ in Fig. 10. The gray curves in panels (a), (c), and (e) join the maxima of the impedance profiles.

by optimal noise levels, while the latter refers to the amplification of the response by an optimal input frequency (f_{res}).

The study of resonance presented in this paper extends the scope of previous work [9–11]. First, we include parameter regimes where the EC cells have stable nodes in addition to stable foci close to the onset of sustained oscillations. The ability of linear systems having stable nodes to exhibit resonance was demonstrated in Refs. [15,16] and the properties of the corresponding impedance and phase profiles was characterized in Ref. [15]. By relaxing the condition of existence of a stable focus to include stable nodes, our concept of resonance is less restrictive than in previous studies [9–12]. Second, we incorporate the study of the phasonant properties

of the EC cell in addition to the standard resonant properties based on the amplitude response. Finally, we incorporate the investigation of the linear mechanisms of generation of both resonance and phasonance in EC cells. These linear mechanisms differ from the mechanisms of generation of resonance/phasonance in linear models. In the former the parameters of the linearized systems contain information about the electrochemical parameters of the original EC cell model, and changes in these parameters generate nonlinear trajectories in the γ_1-γ_2 parameter space. Overall, the theoretical results of this paper predict that resonance and phasonance can be experimentally measured under rather general conditions than previously thought [9,11,12].
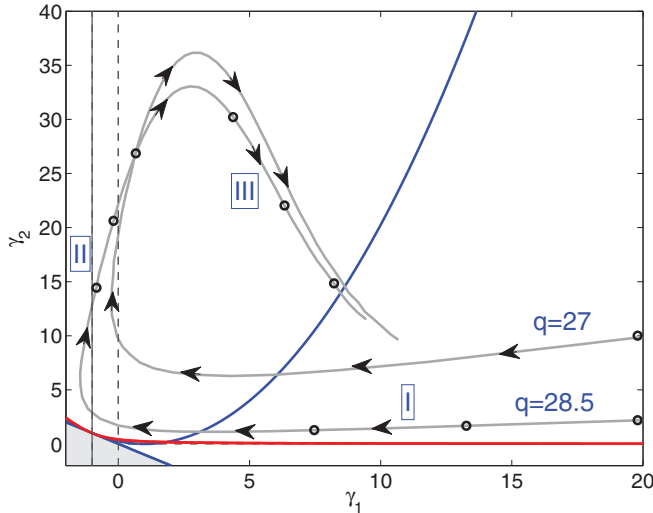
FIG. 12. (Color online) The effect of R on the EC cell linear resonance properties for representative values of q. Trajectories parametrized by R superimposed on the stability/resonant diagrams in γ_1-γ_2 parameter space (arrows indicate increasing values of R). The stability (blue) and resonant (red) curves are as in Fig. 2(c). All trajectories (gray curves) start at $R = 0.1$ outside the range of values of γ_1 ($\gamma_1 > 20$). The points on the trajectories corresponding to $\gamma_1 = 20$ are marked with a black dot. Different trajectories correspond to different values of q. The trajectory for $q = 28.5$ crosses the line $\gamma_1 = -1$ (solid vertical line) and enters the unstable node region (corresponding to limit cycle oscillations) for same range of values of R. We used the following parameters: $\epsilon = 0.03$, $\alpha = 0.1$.

The study of the mechanisms of generation of resonance involves not only the calculation of the resonant and phasonant frequencies and other attributes of the impedance and phase profiles but also the examination of how these attributes change with changes in parameter values. The mapping between the EC cell model parameters and the parameters in the linearized model is complex and not trivial as shown by the nonlinear trajectories in parameter space. In Ref. [15] we have identified three primary mechanisms of generation of resonance that we have briefly reviewed in Sec. III A. These mechanisms are generic for two-dimensional linear systems and describe the generation of resonance and phasonance as the parameters of the linear system change along horizontal (γ_1), vertical (γ_2), and oblique (time-scale separation) lines in γ_1-γ_2 parameter space. However, linear changes in γ_1-γ_2 parameter space do not necessarily reflect the effects of changes in the values of the physicochemical parameters (q, ϵ, R, and α), as shown by Eqs. (15).

In fact, the phase-plane diagrams presented in Sec. III B demonstrate that the fixed points and the corresponding linear properties of the EC cell model (expressed by the linearized parameters γ_1 and γ_2) vary significantly with changes in the physicochemical parameters. The method we used to investigate the linear mechanisms of generation of resonance tracks these changes by generating nonlinear trajectories in γ_1-γ_2 parameter space. By plotting these trajectories on the resonant/stability diagrams (Fig. 2) discussed in Sec. III A and computing the attributes of the impedance and phase profiles along these trajectories (Fig. 3), we uncovered the different

ways in which the physicochemical parameters contribute to the generation of resonance and phasonance and to shape the impedance and phase attributes mentioned above. Our analysis highlights the complex dependence of these attributes with the physicochemical parameters.

Although most of our investigation focused on the dynamics of the linearized EC model, linear and nonlinear effects coexist in our analysis. Specifically, the nonlinear trajectories in γ_1-γ_2 parameter space capture the nonlinearities present in the autonomous EC model (discussed in Sec. III B). These nonlinearities govern the generation of resonance to the linear level in the sense that the path to resonance in the linearized EC model is nonlinear in γ_1-γ_2 parameter space, although for each set of parameter values the model is (obviously) linear.

The model we investigated in this paper is a reduced, caricature model of an EC cell. Although it is based on drastic simplifying assumptions [17] and does not describe the dynamics of an actual EC cell, it captures the relevant physicochemical processes that give rise to the oscillatory behavior observed in realistic EC cells. In addition, the lower dimensionality makes this EC model amenable for analysis using dynamical systems tools. The results obtained and predictions made using reduced models can be then tested in more realistic, higher-dimensional models and in experimental systems.

Reduced and caricature two-dimensional models have been widely used in the literature to investigate nonlinear oscillations in a number of fields, including chemistry, physics, neuroscience, and biology [33]. Prototypical examples include the van der Pol model [34], the FitzHugh-Nagumo model [33, 35–37], the Morris-Lecar model [38], the reduced Oregonator [39], and modified Oregonator [40]. All these models share some geometric and dynamic properties such as the cubiclike shape of the activator nullcline and the time-scale separation between the activator and the inhibitor. The EC model we used here possesses these properties, but the inhibitor (w) nullcline features more complex type of nonlinearities as compared to the reduced models mentioned above.

This study opens various avenues of inquiry about the role of the nonlinearities in shaping the response of EC cells to oscillatory inputs. This include not only parameter sets yielding stable nodes and foci but also stable limit cycles. More research is needed to address these questions and to develop mathematical tools to analyze these issues.

APPENDIX: TWO-DIMENSIONAL LINEAR SYSTEMS: EIGENVALUES, NATURAL FREQUENCY, IMPEDANCE, AND PHASE

We consider the following two-dimensional linear system:

$$
\begin{aligned}
X' &= aX + bY + A_{\text{in}}e^{i\Omega t}, \\
Y' &= cX + dY,
\end{aligned}
\tag{A1}
$$

where a, b, c, and d are constant, $\Omega > 0$, and $A_{\text{in}} \geqslant 0$.
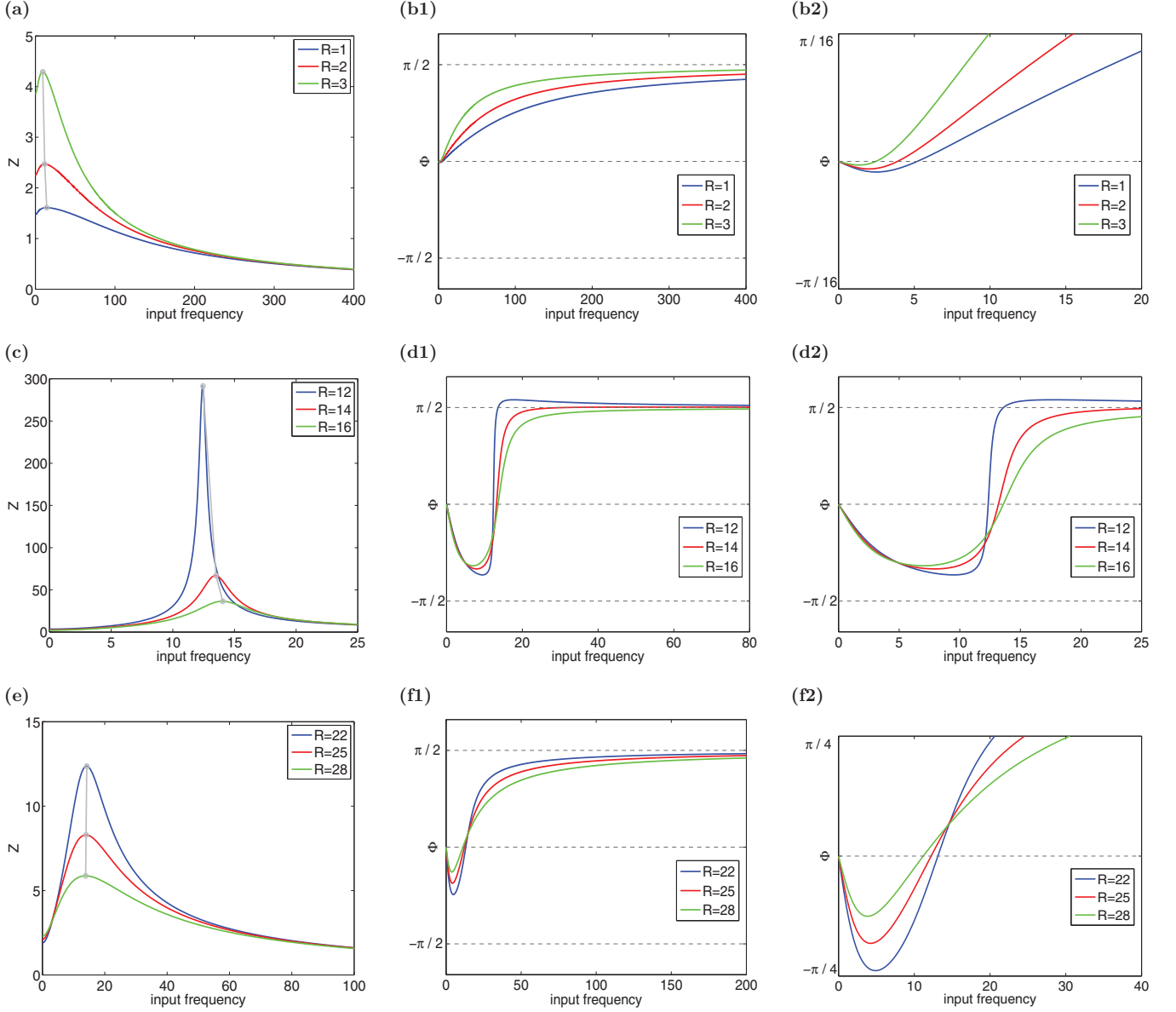
FIG. 13. (Color online) The effect of R on resonance and phasonance properties for the linearized model3 (11) and (12) with $\epsilon = 0.03$, $\alpha = 0.1$, and $q = 28.5$. (a) Impedance profiles on the portion I of the trajectories in Fig. 12. (b) Phase profiles on portion I of the trajectories in Fig. 12. (c) Impedance profiles on portion II of the trajectories in Fig. 12. (d) Phase profiles on portion II of the trajectories in Fig. 12. (e) Impedance profiles on portion III of the trajectories in Fig. 12. (f) Phase profiles on portion III of the trajectories in Fig. 12. The values of R correspond to the black dots on the trajectory for $\alpha = 0.1$ in Fig. 12. The gray curves in panels (a), (c), and (e) join the maxima of the impedance profiles.

1. Intrinsic oscillations and natural frequency

The Jacobian of the corresponding homogeneous system ($A_{\text{in}} = 0$) is given by

$$J = \begin{pmatrix} a & b \\ c & d \end{pmatrix}. \qquad (A2)$$

The roots of the characteristic polynomial are given by

$$r_{1,2} = \frac{(a+d) \pm \sqrt{(a-d)^2 + 4bc}}{2}. \qquad (A3)$$

From Eq. (A3), the homogeneous system displays oscillatory solutions for values of the parameters satisfying

$$4bc + (a-d)^2 > 0 \quad \text{and} \quad ad - bc > 0. \qquad (A4)$$

2. Voltage response to sinusoidal inputs: Impedance amplitude and phase

The particular solutions to system (A1) have the form

$$X_p(t) = A_{\text{out}} e^{i\Omega t} \quad \text{and} \quad Y_p(t) = B_{\text{out}} e^{i\Omega t}. \qquad (A5)$$

Substituting into system (A1) and rearranging terms we obtain

$$\begin{pmatrix} (i\Omega - a) & -b \\ -c & (i\Omega - d) \end{pmatrix} \begin{pmatrix} A_{\text{out}} \\ B_{\text{out}} \end{pmatrix} = \begin{pmatrix} A_{\text{in}} \\ 0 \end{pmatrix}. \quad \text{(A6)}$$

By solving the algebraic system (A6) we obtain the impedance function

$$Z(\Omega) = \frac{A_{\text{out}}}{A_{\text{in}}} = \frac{-d + i\Omega}{(ad - bc - \Omega^2) - i\Omega(a + d)}, \quad \text{(A7)}$$

the impedance amplitude

$$|Z(\Omega)|^2 := \frac{A_{\text{out}}^2}{A_{\text{in}}^2} = \frac{d^2 + \Omega^2}{[ad - bc - \Omega^2]^2 + (a + d)^2\Omega^2}, \text{(A8)}$$

and the phase

$$\phi(\Omega) = \tan^{-1}\frac{(ad - bc - \Omega^2)\,\Omega - (a + d)\Omega d}{(ad - bc - \Omega^2)d + (a + d)\,\Omega^2}. \quad \text{(A9)}$$

3. Dynamics of λ-ω systems

The so-called λ-ω systems [41] have the form

$$\frac{dx}{dt} = -\lambda x - \omega y, \quad \text{(A10)}$$

$$\frac{dy}{dt} = \omega x - \lambda y, \quad \text{(A11)}$$

with $\lambda > 0$ and $\omega > 0$. The alternative formulation in terms of a second-order differential equations reads

$$\frac{d^2x}{dt^2} + 2\lambda\frac{dx}{dt} + (\lambda^2 + \omega^2)x = 0. \quad \text{(A12)}$$

The eigenvalues and natural frequency are given by

$$r_{1,2} = -\lambda \pm \sqrt{-\omega^2} \quad \text{and} \quad \Omega_{\text{nat}} = \omega. \quad \text{(A13)}$$

The resonant and phase-resonant frequencies upon perturbation of Eq. (A10) with a sinusoidal input are given by

$$\Omega_{\text{res}} = \sqrt{-\lambda^2 + \omega\sqrt{4\lambda^2 + \omega^2}} \quad \text{and} \quad \Omega_{\text{phas}} = \sqrt{\omega^2 - \lambda^2}.$$
$$\text{(A14)}$$

For $\lambda = 0$,

$$\Omega_{\text{nat}} = \Omega_{\text{res}} = \Omega_{\text{phas}}. \quad \text{(A15)}$$

System (A10)–(A11) can be transformed into a system of the form (11) and (12) by defining

$$v = \omega x, \quad w = \lambda y, \quad \hat{t} = \lambda t, \quad \text{(A16)}$$

and

$$\gamma_1 = 1, \quad \gamma_2 = \frac{\omega^2}{\lambda^2}, \quad \text{(A17)}$$

4. Oscillatory inputs: Auxiliary calculations

For a sinusoidal input of the form $F(t) = A_{\text{in}}\sin(\Omega t)$, the system's output will be a function,

$$X(t) = A_{\text{out}}\sin(\Omega t - \phi). \quad \text{(A18)}$$

Equation (A18) can be rewritten as follows:

$$X(t) = A_{\text{out}}\cos\phi\sin(\Omega t) - A_{\text{out}}\sin\phi\cos(\Omega t) \quad \text{(A19)}$$

or

$$X(t) = A_{\text{out},1}\sin(\Omega t) + A_{\text{out},2}\cos(\Omega t) \quad \text{(A20)}$$

with

$$A_{\text{out},1} = A_{\text{out}}\cos\phi, \quad A_{\text{out},2} = -A_{\text{out}}\sin\phi. \quad \text{(A21)}$$

Solving for A_{out} and ϕ we obtain

$$A_{\text{out}}^2 = A_{\text{out},1}^2 + A_{\text{out},2}^2 \quad \text{(A22)}$$

and

$$\phi = -\tan^{-1}\left(\frac{A_{\text{out},2}}{A_{\text{out},1}}\right). \quad \text{(A23)}$$

From (A22)

$$Z^2(\Omega) = \frac{A_{\text{out},1}^2 + A_{\text{out},2}^2}{A_{\text{in}}^2}. \quad \text{(A24)}$$

[1] M. T. M. Koper, J. Chem. Soc. Faraday Trans. **94**, 1369 (1998).

[2] M. T. M. Koper, Adv. Chem. Phys. **92**, 161 (1996).

[3] K. Krischer, Mod. Aspects Electrochem. **32**, 1 (1999).

[4] J. Wojtowicz, Mod. Aspects Electrochem. **8**, 47 (1973).

[5] J. L. Hudson and T. T. Tsotsis, Chem. Eng. Sci. **49**, 1493 (1994).

[6] M. T. M. Koper, J. Electroanal. Chem. **409**, 175 (1996).

[7] I. Kiss, V. Gáspár, and L. Nyikos, J. Phys. Chem. A **102**, 909 (1998).

[8] M. Naito, N. Tanaka, and H. Okamoto, J. Chem. Phys **111**, 9908 (1999).

[9] A. Karantonis, E. Bourbos, and D. Koutsaftis, Chem. Phys. Lett. **490**, 69 (2010).

[10] A. Karantonis and D. Karaoulanis, Electrochim. Acta **56**, 4119 (2011).

[11] A. Karantonis and D. Karaoulanis, Electrochim. Acta **78**, 244 (2012).

[12] A. Karantonis, E. Bourbos, and D. Karaoulanis, Electrochim. Acta **87**, 912 (2013).

[13] A. Karantonis, M. Pagitsas, and D. Sazou, Chaos **3**, 243 (1993).

[14] J. R. Macdonald (ed.). *Impedance Spectroscopy* (Wiley, New York, 1987).

[15] H. G. Rotstein and F. Nadim, J. Comp. Neurosci., doi: 10.1007/s10827-013-0483-3.

[16] M. J. E. Richardson, N. Brunel, and V. Hakim, J. Neurophysiol. **89**, 2538 (2003).

[17] A. Karantonis and S. Nakabayashi, Chem. Phys. Lett. **347**, 133 (2001).

[18] P. Parmananda, J. Gerardo, M. Escalera Santos, and K. Showalter, Phys. Rev. E **71**, 031110 (2005).

[19] F. Sagués and I. R. Epstein, Dalton Trans. 1201 (2003).

[20] V. K. Vanag, L. Yang, M. Dolnik, A. M. Zhabotinsky, and I. R. Epstein, Nature, **406**, 389 (2000).

[21] C. M. Gray, J. Comput. Neurosci. **1**, 11 (1994).

[22] E. Marder and R. L. Calabrese, Physiol. Rev. **76**, 687 (1996).

[23] G. Buzsáki. *Rhythms of the Brain* (Oxford University Press, Oxford, 2006).

[24] X. J. Wang, Physiol. Rev. **90**, 1195 (2010).

[25] R. D. Traub and M. A. Whittington. *Cortical Oscillations in Health and Disease* (Oxford University Press, Oxford, 2010).

[26] B. Hutcheon and Y. Yarom, Trends Neurosci. **23**, 216 (2000).

[27] I. Z. Kiss, Y. M. Zhai, and J. L. Hudson, Phys. Rev. E **77**, 046204 (2008).

[28] P. Kaira, P. S. Bodega, C. Punckt, H. H. Rotermund, and D. Drefting, Phys. Rev. E **77**, 046106 (2008).

[29] P. S. Bodega, P. Kaira, C. Beta, D. Krefting, D. Bauer, B. Mirwald-Schulz, C. Punckt, and H. Rotermund, New J. Phys. **9**, 61 (2007).

[30] O. Kortluke, V. N. Kuzovkov, and W. von Niessen, Phys. Chem. Chem. Phys. **6**, 1227 (2004).

[31] J. N. Chazalviel and F. Ozanam, J. Electrochem. Soc. **139**, 2501 (1992).

[32] A. Birzu and K. Krischer, Chaos **20**, 043114 (2010).

[33] J. D. Murray. *Mathematical Biology I: An Introduction* (Springer, Berlin, 2002).

[34] B. van der Pol, Phil. Mag. **2**, 978 (1926).

[35] R. FitzHugh, J. Gen. Physiol. **43**, 867 (1960).

[36] R. FitzHugh, in *Biological Engineering*, edited by H. P. Schwan (McGraw–Hill, New York, 1969), pp. 1–85.

[37] J. S. Nagumo, S. Arimoto, and S. Yoshizawa, Proc. IRE **50**, 2061 (1962).

[38] J. Rinzel and G. B. Ermentrout, in *Methods in Neural Modeling*, 2nd ed,) edited by C. Koch and I. Segev (MIT Press, Cambridge, MA, 1998), pp. 251–292.

[39] J. J. Tyson and P. C. Fife, J. Chem. Phys **73**, 2224 (1980).

[40] L. Yang, M. Dolnik, A. M. Zhabotinsky, and I. R. Epstein, Phys. Rev. E **62**, 6414 (2000).

[41] N. Kopell and L. N. Howard, Stud. Appl. Math. **52**, 291 (1973).